Evidence for a collinear easy-plane magnetic structure of multiferroic $EuFe_3(BO_3)_4$: Spectroscopic and theoretical studies

M. N. Popova,[1] B. Z. Malkin,[2] K. N. Boldyrev,[1] T. N. Stanislavchuk,[3,*] D. A. Erofeev,[1,4] V. L. Temerov,[5] and I. A. Gudim[5]

[1]*Institute for Spectroscopy, Russian Academy of Sciences, 108840 Troitsk, Moscow, Russia*

[2]*Kazan Federal University, 420008 Kazan, Russia*

[3]*Department of Physics, New Jersey Institute of Technology, Newark, New Jersey 07102, USA*

[4]*Moscow Institute of Physics and Technology (State University), 141700 Dolgoprydny, Moscow region, Russia*

[5]*L. V. Kirensky Institute of Physics, Siberian Branch of RAS, 660036 Krasnoyarsk, Russia*

(Received 12 July 2016; revised manuscript received 7 October 2016; published 15 November 2016)

We performed high-resolution polarized optical transmission spectroscopy and theoretical studies of multiferroic $EuFe_3(BO_3)_4$ single crystals in the three phases: paramagnetic $R32$ ($T > T_s = 84$ K) and $P3_121$ ($T_s > T > T_N = 34$ K), and antiferromagnetic ($T < T_N$) ones. The analysis of the spectra reveals interesting details of the magnetic structure, namely, a collinear arrangement of the iron magnetic moments along the C_2 symmetry axis in the ab crystallographic plane of $EuFe_3(BO_3)_4$ below T_N. Spectral signatures of the phase transitions and the spin-phonon interaction are observed and discussed. Reliable crystal-field and exchange-interaction parameters are obtained and used to model the magnetic susceptibility of the compound. The results of detailed calculations of the electric polarization of $EuFe_3(BO_3)_4$ in the $R32$ phase are presented, and mechanisms of the magnetoelectric response are discussed. We detect a strong effect of impurities (that enter the crystal from a flux in the course of the crystal growth) on the structural phase-transition temperature and demonstrate a coexistence of both $R32$ and $P3_121$ phases down to the lowest temperatures in a $EuFe_3(BO_3)_4$ crystal grown with the $Bi_2Mo_3O_{12}$ based flux, due to inhomogeneous distribution of impurity Bi^{3+} ions. Our study can be considered as a demonstration of the abilities of optical spectroscopy in delivering new information on a magnetic compound, even in the case when other methods fail.

DOI: 10.1103/PhysRevB.94.184418

I. INTRODUCTION

Europium iron borate $EuFe_3(BO_3)_4$ belongs to an interesting family of new multiferroics with general formula $RM_3(BO_3)_4$(R = Y, Pr-Er, M = Al, Ga, Fe) that have a noncentrosymmetric trigonal structure of the natural mineral huntite [1]. The structure incorporates helical chains of MO_6 octahedra, running along the trigonal axis c (see Fig. 1. A detailed description of the structure can be found, e.g., in Ref. [2]). Depending on the R and M elements, these compounds possess diverse linear and nonlinear optical [3,4], magnetic, magnetoelectric, magnetoelastic (e.g., [5–11] and references therein), and magnetodielectric [12–14] properties, which, in a combination with excellent thermal and mechanical characteristics and chemical stability, makes them attractive for applications. Aluminum and gallium borates are promising materials for different kinds of lasers, including microchip and self-frequency doubling lasers (see, e.g., [15–17] and references therein). Magnetoelectric, magnetoelastic, and magnetodielectric effects can be used, e.g., for constructing different switches and magnetic memory devices. A large magnetoelectric effect was registered in a number of rare-earth (RE) iron borates below the temperature T_N of an antiferromagnetic ordering ($T_N \sim 30 - 40$ K [5]) [14,18,19]. Gigantic magnetoelectric response has recently been observed in $HoAl_3(BO_3)_4$ [10] and $HoGa_3(BO_3)_4$ [11] at 3 K, its value rapidly decreasing upon increasing the temperature. What is more interesting in view of possible applications, $TbFe_3(BO_3)_4$ [20] and $TbAl_3(BO_3)_4$ [9] demonstrate a considerable quadratic magnetoelectric effect at room temperature, exceeding the one observed in the high-temperature multiferroic $BiFeO_3$ and changing its sign upon rotation of the magnetic field by 90° [9,20].

Thus, magnetoelectric properties of $RM_3(BO_3)_4$ are intriguingly diverse. To understand reasons for this diversity and, possibly, to create a new compound from the family showing a desired magnetoelectric response, a general theory of magnetoelectricity in $RM_3(BO_3)_4$ borates has to be built. The first steps in this direction were undertaken in several recent publications. Zvezdin *et al.* discussed two microscopic mechanisms, namely, the electronic one, when effective magnetic and crystal fields produce the electric dipole moment directly in the electronic $4f$ shells of RE ions, and the ionic one, through displacements of oppositely charged ion sublattices due to electron-deformation interaction [21]. These authors have shown that the field and temperature dependences of the electric polarization induced by a magnetic field in $NdFe_3(BO_3)_4$, $SmFe_3(BO_3)_4$ [21], $PrFe_3(BO_3)_4$ [22], and $TbAl_3(BO_3)_4$ [9] can successfully be modeled using the known magnetic structures of iron borates and crystal-field (CF) parameters obtained from high-resolution broad-band optical spectroscopy measurements and CF calculations. They have also calculated the temperature dependence of the magnetoelectric response of $EuFe_3(BO_3)_4$ [21], for which CF parameters were absent, using wave functions of the free Eu^{3+} ion and average energy intervals between the $^7F_0$ ground state and the $^7F_1$ and $^7F_2$ excited states. Another approach was used by Kurumaji *et al.* who considered the p-d hybridization mechanism of magnetoelectricity to explain the temperature

*stantaras@gmail.com

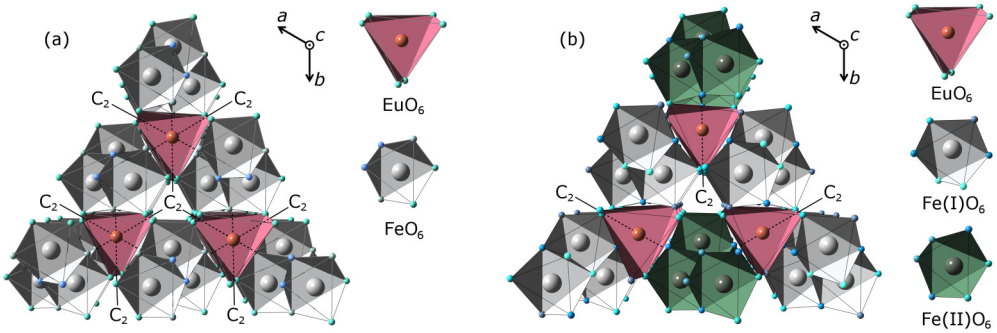

FIG. 1. Distorted triangular EuO_6 prisms surrounded by helical chains of FeO_6 octahedra running along the trigonal axis c of $EuFe_3(BO_3)_4$ in the (a) $R32$ and (b) $P3_121$ crystallographic phases. The site symmetry of the only Eu^{3+} position is D_3 in (a) the $R32$ phase resulting in the three twofold symmetry axes in the ab plane and C_2 in (b) the $P3_121$ phase leading to only one local twofold symmetry axis. There is one Fe^{3+} position in (a) the $R32$ phase but two such positions in (b) the $P3_121$ phase. BO_3 groups are not shown in the figure to retain clarity of the structure.

dependencies of magnetoelectric responses of Gd, Tb, and Eu iron borates [8]. These authors used phenomenological expressions imposed by symmetry, they indicated that to calculate the constants entering these expressions a detailed knowledge of the electronic wave functions and the crystal structure would be needed [8]. Both groups of authors [8,21] addressed $EuFe_3(BO_3)_4$, which seems to be the easiest for interpretation, with its simple singlet ground state of Eu^{3+}, $^7F_0$, separated by a large gap >300 cm^{-1} from the CF levels of the next $^7F_1$ manifold and an available vast information on its magnetic [6,23], and magnetoelectric [6,8] properties. In view of the aforesaid, it is of interest to find reliable CF parameters for $EuFe_3(BO_3)_4$ and to specify its magnetic structure. Having these data in hand it is possible to calculate the values of electric dipole moments induced by a magnetic field both in the electronic $4f$ shell of the RE ion and in the ionic subsystem (due to displacements of oppositely charged ion sublattices in a magnetic field) and, thus, to estimate explicitly contributions of different mechanisms into the magnetoelectric response of the compound. It is worth emphasizing that, in the previous studies [8,21], the field and/or temperature dependencies of magnetoelectric responses of $RM_3(BO_3)_4$ compounds were modeled using adjustable parameters, which did not allow one to make a choice between mechanisms of the magnetoelectric effect.

Like all the other RE iron borates, $EuFe_3(BO_3)_4$ crystallizes in the $R32$ (D_3^7) space symmetry group [1] but, similarly to other compounds $RFe_3(BO_3)_4$ containing RE ions with the ionic radius greater than the one of Sm^{3+}, undergoes a structural phase transition into a less symmetric low-temperature $P3_121(D_3^4)$ phase [2,5,24]. It is worth mentioning that the data on the temperature T_s of the structural phase transition, which is the lowest one among those for the RE iron borates, are controversial; in particular, $T_s = 88$ K [5] and $T_s = 58$ K [25] were reported for powder samples prepared by solid-phase synthesis and for single crystals, respectively. The site symmetry of the only Eu^{3+} position lowers from D_3 in the $R32$ phase to C_2 in the $P3_121$ one. At $T_N = 34$ K, $EuFe_3(BO_3)_4$ orders antiferromagnetically into an easy-plane magnetic structure [6,23]. We note that an arrangement of magnetic moments in the ab plane of the compound remained unclear. Neutron-scattering data on $RFe_3(^{11}BO_3)_4$ (crystals enriched with ^{11}B were grown to avoid a strong neutron absorption by natural boron) revealed collinear arrangements of iron magnetic moments in the ab plane in the cases of $R =$ Y [26], Ho ($T > 5$ K) [26], Er ($T > 10$ K) [27], and Nd ($T > 13.5$ K) [28], whereas a complicated helical and a 120° phase were established for $NdFe_3(BO_3)_4$ below $T_{IC} = 13.5$ K [28] and for $ErFe_3(BO_3)_4$ below 10 K [27], respectively. No magnetic neutron-scattering data exist for $EuFe_3(BO_3)_4$ and it seems to be a problem to carry out magnetic neutron-scattering measurements on $EuFe_3(BO_3)_4$ because both natural boron and natural europium strongly absorb neutrons. Optical spectroscopy is beyond these restrictions. High-resolution spectroscopy of f-f transitions within RE ions in magnetically ordered RE-containing compounds delivers valuable information on the magnetic structure [29]. In some complicated cases it permits one to make a right choice between several spin configurations that are in equally good agreement with the data of neutron experiments. For example, for $Ho_2Cu_2O_5$, four possible models of the magnetic structure were found to fit equally well the neutron-diffraction pattern [30] and the right one has unambiguously been determined with the help of spectroscopic data [31].

In this paper, we communicate data on spectral properties of $EuFe_3(BO_3)_4$ that should be taken into account when developing a microscopic theory of magnetoelectricity in RE iron borates. In particular, on the basis of high-resolution optical spectroscopy studies, we (i) reliably determine energies and symmetries of CF levels of Eu^{3+} in both the high-temperature $R32$ and the low-temperature $P3_121$ phases of $EuFe_3(BO_3)_4$; (ii) perform CF calculations and report reliable CF parameters for both $R32$ and $P3_121$ phases; (iii) reveal the existence of nonequivalent positions for Eu^{3+} ions below T_N and show, on the basis of calculations concerning exchange interactions between the europium and iron ions, that they emerge as a result of a collinear (along the C_2 axis) easy-plane arrangement of Fe^{3+} magnetic moments; (iv) using these results, calculate the electronic and ionic contributions of the Eu^{3+} ions into the electric polarization of $EuFe_3(BO_3)_4$

in the $R32$ phase, induced by a magnetic field; and (v) discuss a dependence of the crystal structure and the temperature T_s of the structural phase transition on a method of the crystal growth and demonstrate a case of a complete suppression of the structural phase transition in $Eu_{0.85}La_{0.15}Fe_3(BO_3)_4$, so that a magnetic ordering takes place in the high-temperature $R32$ phase.

The paper is organized as follows. In Sec. II, we describe the samples used and the details of optical measurements. Section III reports on the optical spectra of $EuFe_3(BO_3)_4$. Spectral signatures of the phase transitions are presented; energies and symmetries of the CF levels of Eu^{3+} in both $R32$ and $P3_121$ phases of paramagnetic europium iron borate are determined; splittings of spectral lines corresponding to singlet-singlet optical transitions below T_N are shown and discussed. Section IV deals with structural peculiarities of $EuFe_3(BO_3)_4$ crystals connected with growth methods. Section V is devoted to a theoretical consideration. The paper ends with the Conclusion.

II. EXPERIMENTAL DETAILS

The $EuFe_3(BO_3)_4$ single crystals were grown by solution-melt technique [32] using two different fluxes, namely, the (i) $Bi_2Mo_3O_{12}$ and (ii) Li_2WO_4 based ones. The solution-melt based on the lithium tungstate was used to avoid the impurities of bismuth ions, which can enter the crystal in the course of a crystal growth process by the solution-melt method [33]. In addition, $Eu_{1-x}La_xFe_3(BO_3)_4$, $x = 0.05$ and 0.15, single crystals were grown from Li_2WO_4 based melt solution. The crystals were of about $3 \times 3 \times 4$ mm^3 in size and of a good optical quality. The space group, lattice constants, and orientation of the axes in the studied crystals were obtained with a SMART APEXII diffractometer (Mo K_α, $\lambda = 0.7106$ Å) at room temperature. All the crystals were single phase, possessed the trigonal $R32$ space symmetry group, and had the structure of the huntite mineral [1,2]. The following lattice parameters were found: $a = 9.5690(9)$ Å, $c = 7.5884(7)$ Å and $a = 9.586(2)$ Å, $c = 7.609(2)$ Å for $EuFe_3(BO_3)_4$ grown with the $Bi_2Mo_3O_{12}$ based flux and for $Eu_{0.85}La_{0.15}Fe_3(BO_3)_4$, respectively. In the case of $RFe_3(BO_3)_4$ crystals grown with the Li_2WO_4 based flux, the lattice parameters were determined for $TbFe_3(BO_3)_4$; they turned out to be equal to those found for the compound prepared by solid-phase synthesis [5]. We believe that the same is true for $EuFe_3(BO_3)_4$. Samples for optical measurements were cut either perpendicular or parallel to the c axis and polished. The 0.1–1-mm-thick samples were used for measurements in different spectral regions. Their orientation was additionally checked by optical polarization methods. Far-infrared spectroscopy measurements with a Bruker IFS 125 HR Fourier spectrometer confirmed that the samples were single phase.

Transmission spectra of the europium iron borate were registered in a wide spectral (30–200 and 900−23000 cm^{-1}) and temperature (3.5–300 K) ranges using a Fourier spectrometer Bruker IFS 125 HR and a closed helium-cycle cryostat Cryomech ST403. The spectra in the π ($\mathbf{k} \perp c$, $\mathbf{E} \parallel c$, $\mathbf{H} \perp c$), σ ($\mathbf{k} \perp c$, $\mathbf{E} \perp c$, $\mathbf{H} \parallel c$), and α ($\mathbf{k} \parallel c$, $\mathbf{E}$, $\mathbf{H} \perp c$) polarizations were studied. Such a complete set of polarizations enabled us to unambiguously identify all the observed spectral lines.

III. OPTICAL SPECTRA OF $EuFe_3(BO_3)_4$: CRYSTAL-FIELD LEVELS AND SIGNATURES OF THE PHASE TRANSITIONS

A. Spectral signatures of phase transitions in $EuFe_3(BO_3)_4$

Figure 2 presents examples of the Eu^{3+} absorption spectra in $EuFe_3(BO_3)_4$ for different polarizations. The spectra change abruptly at the structural phase transition, exhibiting marked shifts and, in some cases, splitting of spectral lines and appearance of new lines below $T_s = 84$ K. Intensity maps of Figs. 2(d), 2(f), and 2(h) illustrate abruptness of changes the most clearly. The changes in the electronic spectra are, evidently, connected with a change of the crystal-field strength and symmetry at the $R32 \rightarrow P3_121$ "weak first-order" [24] phase transition, which induces abrupt changes of the lattice [6,34] and dielectric [6,12,13] constants. A strong impact of this transition on the spectra of infrared-active phonons of $EuFe_3(BO_3)_4$ was revealed in Ref. [25]. Similar results were obtained for Raman [24] and infrared [35] phonon spectra of terbium and gadolinium iron borates. Figure 3 shows a part of the IR phonon spectrum of the same $EuFe_3(BO_3)_4$ sample, electronic spectra of which are presented in Fig. 2. Abrupt shifts of phonon lines and appearance of new phonons below $T_s = 84$ K can be seen (compare with Fig. 1 of Ref. [25] where such changes occurred at $T_s = 58$ K). Shifts and splittings of electronic and phonon spectral lines and emergence of new lines in the spectra of $EuFe_3(BO_3)_4$ start abruptly at the structural phase transition, thus clearly indicating its temperature T_s.

One more critical point is at the temperature of an antiferromagnetic ordering $T_N = 34$ K. No new lines appear in the phonon spectrum, which testifies to an absence of one more structural phase transition at T_N (in contrast to NiB_2O_6, where an antiferromagnetic ordering is accompanied by a structural phase transition [36]). However, phonon frequency versus temperature dependencies exhibit a pronounced peculiarity at T_N [see Fig. 3(c)], indicating a spin-phonon interaction in this multiferroic compound. As for the electronic Eu^{3+} spectra, peculiarities in the line frequencies and additional splitting of some spectral lines are observed [see Figs. 2(e)–2(h)]. To extract more information from this observation, line identification is necessary.

B. Crystal-field levels of Eu^{3+} in the $R32$ and $P3_121$ phases of paramagnetic $EuFe_3(BO_3)_4$

Inspecting optical transitions from the ground state to CF sublevels of excited multiplets (Fig. 2 shows some examples of the spectra) and consulting the selection rules [Table I; $\Gamma_1(\gamma_1)$ and $\Gamma_2(\gamma_2)$ are one-dimensional irreducible representations of the $D_3(C_2)$ point symmetry group, Γ_3 is a two-dimensional one] we were able to unambiguously identify all the observed spectral lines in both the high-temperature $R32$ phase and the low-temperature $P3_121$ one.

The $^7F_0$ ground state of the Eu^{3+} ion is a totally symmetric singlet $\Gamma_1(\gamma_1)$ in the $D_3(C_2)$ group. Γ_3 non-Kramers doublets of the $R32$ phase split into $\gamma_1 + \gamma_2$ singlets of the $P3_121$ phase below the temperature T_s of the structural phase transition. Singlets of the $R32$ phase transform as follows: $\Gamma_1 \rightarrow \gamma_1$ and $\Gamma_2 \rightarrow \gamma_2$, selection rules being relaxed. In particular,

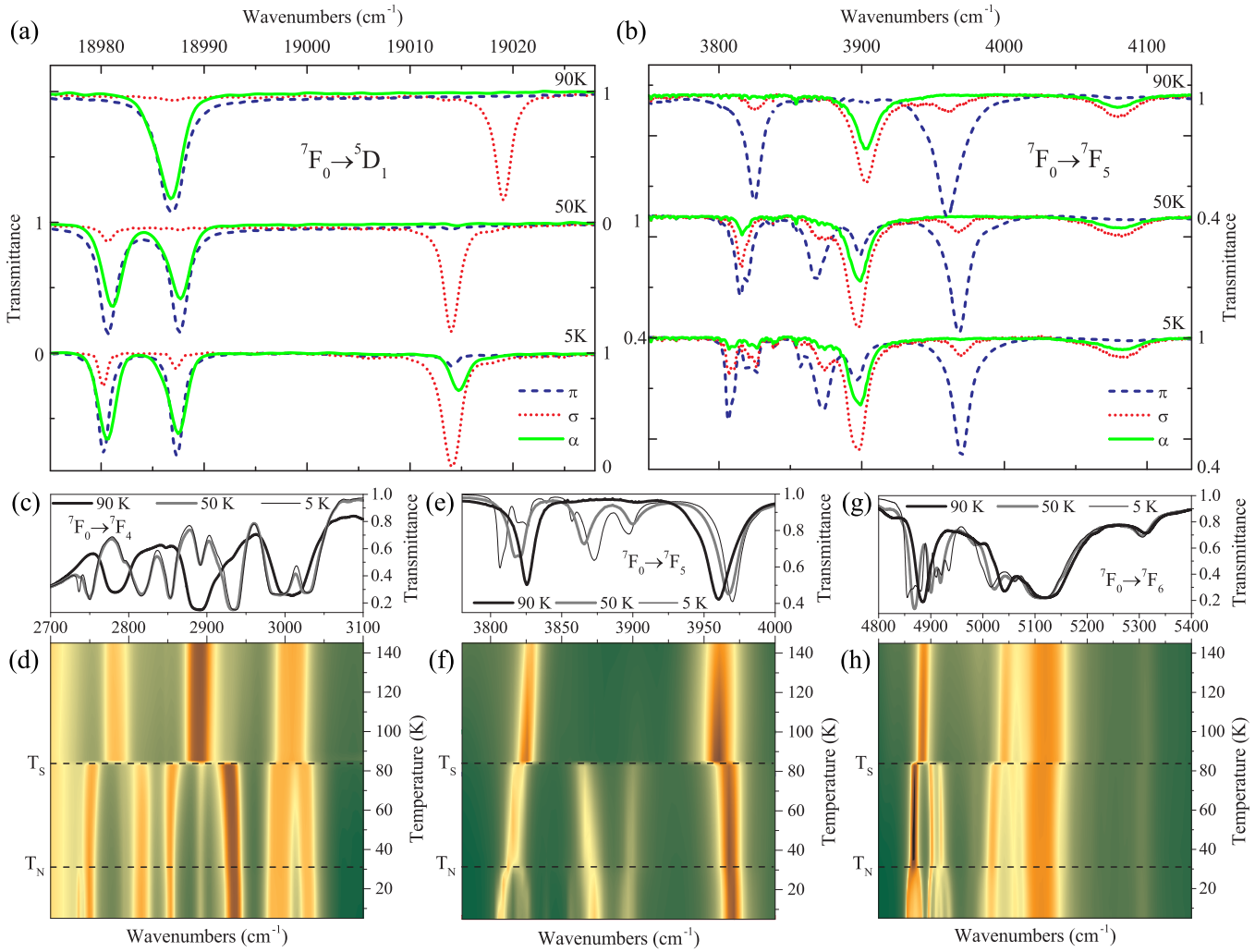

FIG. 2. Transmission spectra of $EuFe_3(BO_3)_4$, corresponding to optical transitions in the Eu^{3+} ion, from the $^7F_0$ singlet ground state to (a) $^5D_1$, (b),(e),(f) $^7F_5$, (c),(d) $^7F_4$, and (g),(h) $^7F_6$, (a),(b) in the π (blue dashed lines), σ (red dotted lines), and α (green solid lines) polarizations for three representative temperatures: $T = 90\ \mathrm{K} > T_s$, $T_s > T = 50\ \mathrm{K} > T_N$, and $T = 5\ \mathrm{K} < T_N$; (c),(d),(g),(h) σ and (e),(f) π polarized spectra, presented as (c),(e),(g) transmittance at 90 K (black thick lines), 50 K (gray thick lines), and 5 K (black thin lines) and (d),(f),(h) intensity maps.

strictly forbidden in the $R32$ phase $\Gamma_1 \rightarrow \Gamma_1$ optical transitions become allowed in the $P3_121$ phase for α and σ (α and π) polarizations as electric dipole (magnetic dipole) ones; absence by symmetry reasons of $\Gamma_1 \rightarrow \Gamma_2$ transitions in the α polarization no more holds valid for the $P3_121$ phase (see Table I).

Using these selection rules we can confidently assign the observed spectral lines, indicate the nature of the optical transition, and interpret changes at phase transitions in $EuFe_3(BO_3)_4$. For example, in Fig. 2(a), $T = 90\ \mathrm{K} > T_s$, presenting optical transitions to the $^5D_1(\Gamma_3 + \Gamma_2)$ CF multiplet, both observed lines are of the magnetic dipole nature, the high-frequency one corresponds to the $\Gamma_1 \rightarrow \Gamma_2$ transition (it is absent in the α polarization). The low-frequency $\Gamma_1 \rightarrow \Gamma_3$ line splits into two lines, $\gamma_1 \rightarrow \gamma_1 + \gamma_2$ at the $R32 \rightarrow P3_121$ phase transition. We note a downward shift of the center of gravity of the $^5D_1$ level (and, in fact, of the whole ^5D term) in the $P3_121$ phase, that gives evidence for an expansion of the $4f^6$ electronic shell of the Eu^{3+} ions in this low-symmetry phase (nephelauxetic effect). Experimental data on the CF levels in both $R32$ and $P3_121$ crystallographic phases of $EuFe_3(BO_3)_4$ are collected in Table II. It is worth mentioning that the experimentally observed splittings of different Γ_3 levels at the $R32 \rightarrow P3_121$ phase transition differ by more than an order of magnitude (see Table II).

An additional splitting observed at T_N [see Figs. 2(b), 2(f), and 2(h)] deserves special consideration.

C. Splitting of Eu^{3+} spectral lines in a magnetically ordered state of $EuFe_3(BO_3)_4$

In the $R32$ phase, magnetic moments of the Eu^{3+} ions in the Γ_3 states are directed along the c axis of the crystal, but in the $P3_121$ phase, these moments not only change their values but also deviate from the c axis in local yz planes perpendicular to the local axes $x||C_2$. From the analysis of temperature dependences of components of the magnetic dc-susceptibility tensor, it follows that magnetic moments of the

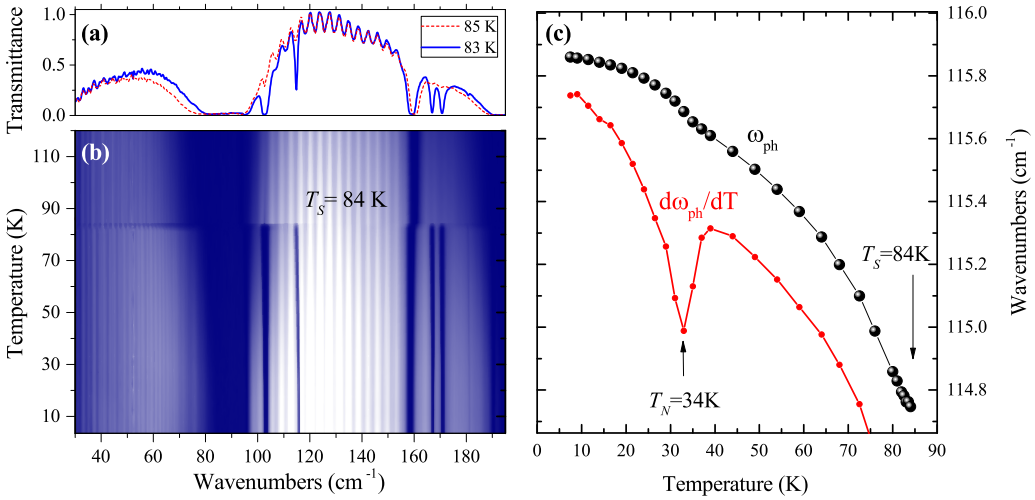

FIG. 3. Far-infrared spectral signatures of the phase transitions in $EuFe_3(BO_3)_4$. (a),(b) α polarized far-infrared spectra represented as (a) transmittance at 85 K $> T_s = 84$ K (red dashed line) and 83 K $< T_s$ (blue solid line) and (b) intensity map. Appearance of new phonon lines at $T_s = 84$ K announces a symmetry lowering at the structural phase transition. (c) Frequency vs temperature dependence (symbols; the solid line is a guide for the eye) and its derivative (lower red trace) for a new phonon mode near 115 cm^{-1}. Error bars are within dimensions of the symbols. Peculiarity at $T_N = 34$ K testifies the spin-phonon coupling.

Fe^{3+} ions in a magnetically ordered $EuFe_3(BO_3)_4$ crystal lie in the *ab* plane [23]. If the magnetic structure were collinear along one of the three C_2 axes, there would be two magnetically nonequivalent subsystems of the Eu^{3+} ions, with the ratio 1:2 for the number of ions in each of them. For ions of the first subsystem, the effective exchange field is parallel to the local $x||C_2$ axis, whereas for ions of the second subsystem, this field forms the angles $\pm 2\pi/3$ with the x axes (and angles $\frac{-5\pi}{6}$ and $\frac{-\pi}{6}$ with the local y axes, respectively). Thus, in the case of a collinear easy-plane magnetic structure, one could await a doubling of the number of spectral lines, with the ratio of integral intensities 1:2.

Indeed, the lowest-frequency lines (not broadened by phonon relaxation) of the $^7F_5$ and $^7F_6$ optical multiplets demonstrate a splitting into two or more components below T_N [see Figs. 2(e)–2(h) and Table III]. The ratio 1:2 for integral intensities is fulfilled within experimental error limits (Fig. 4). This experimental observation strongly suggests a collinear structure of the iron magnetic moments in the *ab* plane. As we'll see in Sec. V, the observed splittings are in qualitative agreement with the calculated ones.

TABLE I. Selection rules for the electric dipole (ED) and magnetic dipole (MD) transitions of a non-Kramers ion in the D_3 and C_2 positions. The axes *x, y, z* of a local Cartesian system of coordinates are oriented relative to the crystal axes *a, b, c* in the following way: $z||c$, $x||a||C_2$, $y\perp a$. Allowed components of the ED (MD) moment are denoted as d_i (μ_i), $i = x, y, z$, respectively.

	ED			MD		
D_3	Γ_1	Γ_2	Γ_3	Γ_1	Γ_2	Γ_3
Γ_1		d_z	d_x,d_y		μ_z	μ_x,μ_y
		π	α,σ		σ	α,π
Γ_2	d_z		d_x,d_y	μ_z		μ_x,μ_y
	π		α,σ	σ		α,π
Γ_3	d_x,d_y	d_x,d_y	d_x,d_y,d_z	μ_x,μ_y	μ_x,μ_y	μ_x,μ_y,μ_z
	α,σ	α,σ	α,σ,π	α,π	α,π	α,σ,π
C_2	γ_1	γ_2		γ_1	γ_2	
γ_1	d_x	d_z,d_y		μ_x	μ_z,μ_y	
	α,σ	α,σ,π		α,π	α,σ,π	
γ_2	d_z,d_y	d_x		μ_z,μ_y	μ_x	
	α,σ,π	α,σ		α,σ,π	α,π	

IV. SUPRESSION OF THE $R32 \rightarrow P3_121$ PHASE TRANSITION IN THE $Eu_{0.85}La_{0.15}Fe_3(BO_3)_4$ CRYSTAL

Hinatsu *et al.* [5] have established a linear dependence of the temperature T_s of a structural phase transition on the ionic radius of the RE ion in RE iron borates (see Fig. 7 in Ref. [5]). The authors of Ref. [5] studied powder samples prepared by solid-state reaction. Interestingly, T_s reported for single crystals of $RFe_3(BO_3)_4$, $R = Y, Er - Eu$ [24,25], always was lower than T_s of Ref. [5]. What is important, $RM_3(BO_3)_4$ crystals are grown by solution-melt methods using different fluxes [1,32,33]. In particular, large crystals of good optical quality are obtained with the $Bi_2Mo_3O_{12}$ based flux [32]. Earlier, we have supposed that lower T_s for single crystals are connected with entering of a "big" Bi^{3+} ion from the flux into positions of R^{3+} ions, which increases the "effective" ionic radius of the RE ion and, thus, lowers T_s [37]. A direct spectroscopic proof of Bi^{3+} entering into $RAl_3(BO_3)_4$ crystals has been demonstrated in Ref. [33].

We have compared optical spectra of $EuFe_3(BO_3)_4$ crystals grown by solution-melt technique using (i) $Bi_2Mo_3O_{12}$ and (ii) Li_2WO_4 based fluxes. The spectra clearly evidence $T_s = 58$ K for the sample (i) (see Fig. 1 of Ref. [25]) and $T_s = 84$ K for the (ii) one (see Fig. 3) whereas $T_N = 34$ K for both samples. We note that $T_s = 84$ K observed for sample (ii) is close to $T_s = 88$ K reported for powder samples prepared by solid-phase synthesis [5]. An estimate based on the dependence established in Ref. [5] (see Fig. 5), gives $5 \pm 1\%$ for the Bi concentration in the sample (i). Here, we used

TABLE II. Energies $E(\mathrm{cm}^{-1})$ of CF levels of Eu^{3+} in paramagnetic $EuM_3(BO_3)_4$ borates and shifts $\Delta E = E(P3_121) - E(R32)$ induced by the structural phase transition $R32 \rightarrow P3_121$ in $EuFe_3(BO_3)_4$. In columns 2 and 7, irreducible representations are indicated for the $R32$ and $P3_121$ point symmetry groups, respectively. In column 4, electric dipole (e) or magnetic dipole (m) nature of the optical transition from the ground state is indicated.

$^{2S+1}L_J$	Symmetry in the $R32$ phase	M = Al, $E(R32)$ [45]	M = Fe, $E(R32)$ (T = 88 K)		M = Fe, $E(P3_121)$ (T = 80 K) $\Delta E = E(P3_121) - E(R32)$			
			Measured	Calc.	Measured[a]		Calc., $\gamma_i, \Delta E$	
1	2	3	4	5	6		7	
$^7F_0$	Γ_1	0	0	0	0		γ_1 0	
$^7F_1$	Γ_3	323	325	331.5	318 (−7)	342 (17)	γ_2 −13.8,	γ_1 13.2
	Γ_2	453	445	447.4			γ_2 0.8	
$^7F_2$	$1\Gamma_3$	931		951.9			γ_2 −2.1,	γ_1 2.4
	$2\Gamma_3$	1049		1046.8			γ_2 −6.0,	γ_1 4.2
	Γ_1			1225.6			γ_1 3.7	
$^7F_3$	$1\Gamma_2$	1821	1840 e	1836.7	1840 (0)		γ_2 0.7	
	Γ_1			1886.5			γ_1 −1.5	
	$1\Gamma_3$	1939	1919 e	1923.9	1913 (−6)	1920 (1)	γ_1 −2.8,	γ_2 1.9
	$2\Gamma_3$	1965	1940 e	1950.9		1944 (4)	γ_2 −7.0,	γ_1 8.2
	$2\Gamma_2$	2063[b]	1961 e	1961.5	1958 (−3)		γ_2 2.3	
$^7F_4$	$1\Gamma_1$			2734.5	2735		γ_1 0	
	$1\Gamma_3$	2536[b]	2782 e	2773.9	2754(−28)	2816 (34)	γ_2 −16.5,	γ_1 17.9
	$2\Gamma_3$	2596[b]	2889 e	2894.9	2855(−34)	2929(40)	γ_1 −26.0,	γ_2 25.1
	Γ_2	2907	2892 e	2928	2892(0)		γ_2 2.1	
	$2\Gamma_1$			3007			γ_1 −1.3	
	$3\ \Gamma_3$	3009	3009 e,m	3008.8	2997 (−12)	3025 (15)	γ_2 −1.0,	γ_1 6.6
$^7F_5$	$1\Gamma_2$		3825 e,m	3819.3	3819 (−6)		γ_2 −6.0	
	$1\Gamma_3$		3831	3828.4	3821(−10)		γ_2 −7.4,	γ_1 6.9
	$2\Gamma_3$		3854	3854.9		3865(11)	γ_2 0.2,	γ_1 5.1
	$3\Gamma_3$		3903 e	3898.2	3899 (−4)		γ_1 −3.0,	γ_2 2.3
	$2\Gamma_2$	3997	3960 e,m	3979.5	3966 (6)		γ_2 6.2	
	Γ_1			4037.7			γ_1 2.4	
	$4\Gamma_3$	4092	4079 e	4079.4		4081 (2)	γ_2 1.5,	γ_1 3.1
$^7F_6$	$1\Gamma_3$	4863	4884 e	4889.5	4869 (−15)		γ_2 −11.1,	γ_1 −9.3
	$1\Gamma_1$			4890.7	4900		γ_1 12.0	
	$1\Gamma_2$	4905	4906 e	4907.9	4917 (11)		γ_2 5.2	
	$2\Gamma_3$	4893		4916.7			γ_1 1.3,	γ_2 5.1
	$2\Gamma_1$			5044			γ_1 2.1	
	$3\Gamma_3$	5087[b]	5041 e	5047.2	5023 (−18)	5057 (16)	γ_2 −15.4,	γ_1 19.8
	$4\Gamma_3$	5166[b]	5120 e	5108.7	5114 (−6)		γ_2 1.5,	γ_1 4.4
	$2\Gamma_2$	5353	5316 e,m	5291.8	5308 (−8)		γ_2 2.2	
	$3\Gamma_1$			5291.9			γ_1 2.2	
$^5D_0$	Γ_1	17215		17242	17236		γ_1 0	
$^5D_1$	Γ_3	18965	18987 m	18986	18982 (−5)	18988 (1)	γ_2 −3,	γ_1 4
	Γ_2	19001	19019 m	19023	19015 (−4)		γ_2 1	
$^5D_2$	Γ_1	21415		21448	21450		γ_1 1	
	$1\Gamma_3$	21418	21454 e	21459	21454 (0)	21455 (1)	γ_1 0,	γ_2 1
	$2\Gamma_3$	21489	21510 e	21501	21504(−6)	21508(−2)	γ_1 −3,	γ_2 4

[a]Shifts ΔE are in parentheses.

[b]Positions of CF levels of Eu^{3+} ions in $EuAl_3(BO_3)_4$ to be checked.

the following relation for the "effective" ionic radius of the RE ion in a "mixed" compound $R_{1-x}Bi_xFe_3(BO_3)_4$: $r_{\mathrm{eff}} = (1-x)\,r_{\mathrm{Eu}} + x r_{\mathrm{Bi}}$, with $r_{\mathrm{Eu}} = 0.947$ Å, $r_{\mathrm{Bi}} = 1.030$ Å [38]. In a similar way, we have evaluated the Bi^{3+} concentration in a number of RE iron borate crystals grown with a Bi-containing flux. In all investigated materials (R = Dy, Ho, Tb, Gd), the concentration of bismuth was in the range 5–7%.

As $EuFe_3(BO_3)_4$ has the lowest T_s temperature of the structural $R32 \rightarrow P3_121$ phase transition, it seemed possible to completely suppress the transition by producing a sample with the Bi concentration of about 12%. We failed, however, to grow such crystal and decided to replace Bi^{3+} by La^{3+}, which has almost the same ionic radius as Bi^{3+}, $r_{\mathrm{La}} = 1.032$ Å [38], but chemically is close to Eu^{3+} (note that $LaFe_3(BO_3)_4$ crystallizes in the trigonal $R32$ huntite structure [1], whereas a $BiFe_3(BO_3)_4$ compound with a trigonal structure is not known). To avoid any contribution on suppression of transition temperature T_s coming from

TABLE III. Energy levels (cm^{-1}) of Eu^{3+} in the magnetically ordered phase of $EuFe_3(BO_3)_4$ and shifts of energy levels $\Delta E = E(T = 5\ K) - E(T_N)$. M_{Fe} is the magnetic moment of the Fe^{3+} ions.

					Calculated shifts of energy levels				
					EuII ($M_{Fe,x} = -M_{Fe}/2$, $M_{Fe,y} = \pm\sqrt{3}M_{Fe}/2$)			EuI ($M_{Fe} \| x$)	
Multiplet 1	Symmetry in the $R32$ phase 2	Measured energy levels, $E(T = 5\ K)$, and shifts ΔE (in parentheses) 3			4			5	
$^7F_3$	Γ_2		1840 (0)			0.3			0.2	
	Γ_1		1884			0.2			0.2	
	$1\Gamma_3$	1913 (0)		1920 (0)	−0.9		−0.1	−0.2		−1.7
	$2\Gamma_3$	1942		1947 (3)	1.3		−1.1	1.9		1.1
	Γ_2		1959 (1)			2.8			0.7	
$^7F_4$	Γ_1		2736.5 (−0.2)			−0.5			−0.2	
	$1\Gamma_3$	2751 (1)		2816 (0)	0.8		0.2	0.2		0.3
	$2\Gamma_3$	2853.4 (0)		2935.6 (1)	0.2		0.3	0.5		−0.5
	Γ_2		2892 (0)			0.2			0.6	
	Γ_1		2986 (−3)			−3.2			−2.1	
	$3\Gamma_3$	2995 (1)		3030 (1)	3.2		1.7	0.9		2.9
$^7F_5$	$1\Gamma_2$	3806.5 (−5.3)		3810.2 (−1.6)[a]		−3.8			−7.1	
	$1\Gamma_3$	3818.5		3821.2		1.5			7.3	
		3824.1		3826.8[a]		1.2			−0.4	
	$2\Gamma_3$	3839				−0.3			0.3	
		3857		3873 (5)		1.5			0.4	
	$3\Gamma_3$	3894 (−3)		3898 (1)	0.3		0.9	0.8		0.2
	$2\Gamma_2$		3970 (1)			0.7			0.5	
	Γ_1					−0.4			−0.8	
	$4\Gamma_3$		4086 (5)		0.7		1.2	1.6		0.6
$^7F_6$	$1\Gamma_3$	4855.2 (−8.1)		4863.3 (0)[a]		−9.2			−0.3	
		4871.4 (−2)		4880.7 (7.3)[a]		7.2			−1.1	
	$1\Gamma_1$	4895 (−4)		4899.3 (0.5)[a]		−1.9			−3.5	
	$1\Gamma_2$	4907 (−7)		4911 (−3)[a]		−2.2			−6.2	
	$2\Gamma_3$	4920		4935	2.1		5.8	5.4		7.3
	$2\Gamma_1$					3.9			−4.0	
	$3\Gamma_3$	5016 (−2)		5061 (2)	−4.7		0.8	−0.1		3.2
	$4\Gamma_3$	5114 (0)			1		0.9	0.7		1.8
	$2\Gamma_2$		5307 (0)			0.1			0.5	
	$3\Gamma_1$					0.9			0.5	
$^5D_0$	Γ_1		17235 (−1)			1			1	
$^5D_1$	Γ_3	18980		18987	0		0	0		0
	Γ_2		19014			1			0	
$^5D_2$	Γ_1					−1			−1	
	$1\Gamma_3$				0		0	1		0
	$2\Gamma_3$				1		1	1		1

[a]From the decomposition of the spectrum envelope into components (see Fig. 4).

Bi impurities, $Eu_{1-x}La_xFe_3(BO_3)_4$ crystals were grown with the Li_2WO_4 based flux. The $Eu_{0.95}La_{0.05}Fe_3(BO_3)_4$ crystal grown in such way demonstrated a very sharp (<0.5 K) transition with the same $T_s \approx 58$ K as $EuFe_3(BO_3)_4$ crystals grown with the $Bi_2Mo_3O_{12}$ based flux. In the $Eu_{0.85}La_{0.15}Fe_3(BO_3)_4$ crystal, the structural transition was completely suppressed. Figure 6(a) shows the temperature evolution of its spectrum, with a clearly visible magnetic ordering in the $R32$ high-symmetry crystallographic phase and no trace of the $R32 \rightarrow P3_121$ structural phase transition [compare with Fig. 6(b) for $EuFe_3(BO_3)_4$]. Thus, a possibility is demonstrated to control the temperature of a structural phase transition in an iron borate crystal, which could be useful in certain applications (e.g., sensors, switches).

We have also found out that a presence of the Bi impurity in a europium iron borate crystal may strongly modify its properties. Figure 7 illustrates this. While in a crystal grown with the Li_2WO_4 based flux (having $T_s = 84$ K) clear spectral signatures of both structural and magnetic phase transitions are evident, in a crystal grown with the $Bi_2Mo_3O_{12}$ based flux ($T_s = 58$ K) a lot of extra lines are present. A majority of them can be interpreted as a superposition of the spectra for $R32$ and $P3_121$ phases, which shows that a considerable part of the crystal remains in the $R32$ phase even at 5 K,

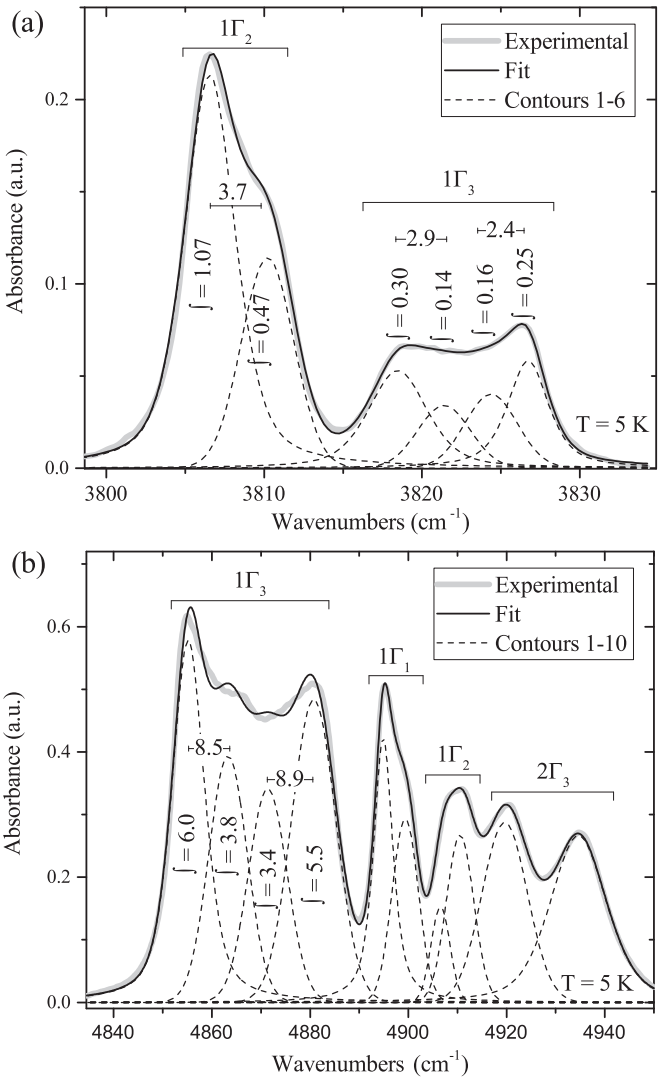

FIG. 4. Decomposition of the low-temperature Eu^{3+} absorption lines (a) ${}^7F_0(\Gamma_1) \rightarrow {}^7F_5(1\Gamma_2, 1\Gamma_3)$ and (b) ${}^7F_0(\Gamma_1) \rightarrow {}^7F_6(1\Gamma_3, 1\Gamma_1, 1\Gamma_2, 2\Gamma_3)$ into components that originate from magnetically nonequivalent europium positions in the case of a collinear arrangement of iron magnetic moments along one of the C_2 axes in the ab plane.

evidently, due to inhomogeneous distribution of Bi impurities in the crystal. More additional extra lines in this crystal come from Eu^{3+} ions located near Bi impurities. To summarize, one should be very careful when interpreting optical, magnetic, and magnetoelectric properties of functional RE borate materials, taking into account their growth-method-dependent structural peculiarities.

V. THEORY AND SIMULATIONS

The Hamiltonian of the Eu^{3+} ions in a paramagnetic $EuFe_3(BO_3)_4$ crystal reads

$$H = H_{\mathrm{FI}} + H_{\mathrm{CF}}(D_3), \tag{1}$$

for the case of the high-temperature ($T > T_s$) $R32$ phase, in which Eu^{3+} is subjected to a trigonal crystal field of the D_3

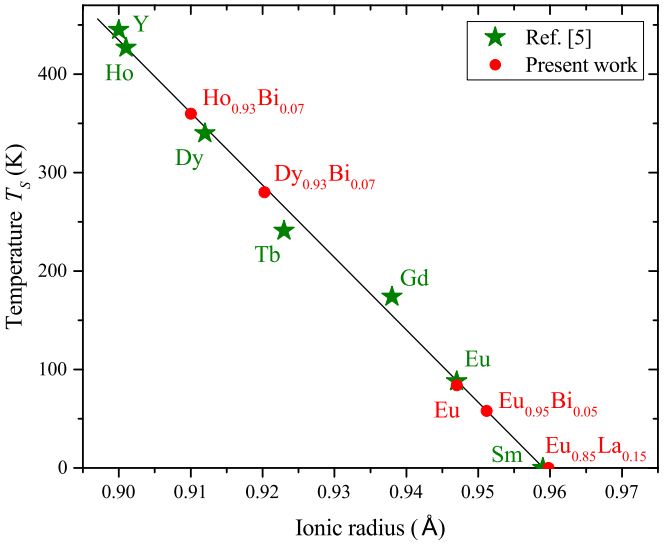

FIG. 5. The temperature of the structural phase transition T_s in $RFe_3(BO_3)_4$ vs ionic radius of R^{3+}. Stars and solid line: data of Ref. [5] for powder samples obtained by solid-phase synthesis. Filled circles: our data on the $RFe_3(BO_3)_4$ crystals grown with a Bi-containing flux, which reveal the Bi concentration in the sample, and on the $Eu_{1-x}La_xFe_3(BO_3)_4$ ($x = 0$ and 0.15) crystals grown with the Li_2WO_4 based flux [$r_{\mathrm{eff}} = (1-x)r_{\mathrm{Eu}} + xr_{\mathrm{La}}$].

symmetry, or

$$H = H_{\mathrm{FI}} + H_{\mathrm{CF}}(D_3) + \Delta H_{\mathrm{CF}}(\mathrm{C}_2), \tag{2}$$

for the case of the low-temperature $P3_121$ phase ($T_s > T > T_N$, the symmetry of the crystal field is C_2).

Below the temperature T_N of an antiferromagnetic ordering of iron magnetic moments in the crystallographic ab plane,

$$H = H_{\mathrm{FI}} + H_{\mathrm{CF}}(D_3) + \Delta H_{\mathrm{CF}}(\mathrm{C}_2) + H_{fd}. \tag{3}$$

The H_{fd} operator in Eq. (3) is responsible for a change of the spectrum of the Eu^{3+} ions due to exchange interaction with the nearest Fe^{3+} ions.

In Eqs. (1)–(3), the operator H_{FI} corresponds to the energy of the free ion, which includes the energy of the electrostatic interaction between $4f$ electrons of the $4f^6$ shell, the energy of the spin-orbit coupling, and also terms corresponding to an interaction between different configurations and to additional relativistic spin-spin and spin-orbit interactions. We use the standard form of this operator [39] defined in the total space of 3003 states of the electronic $4f^6$ configuration:

$$H_{\mathrm{FI}} = \zeta \sum_j \boldsymbol{l}_j \boldsymbol{s}_j + \alpha L(L+1) + \beta \hat{G}(G_2) + \gamma \hat{G}(R_7) + \sum_k (F^k \hat{f}_k + P^k \hat{p}_k + T^k \hat{t}_k + M^k \hat{m}_k), \tag{4}$$

where the sum in the first term at the right-hand side is taken over six $4f$ electrons with angular moments l_j and spin moments s_j. In the calculations, we used the parameters of the electrostatic interaction between the $4f$ electrons $F^2 = 82031, F^4 = 59133, F^6 = 42699$; the spin-orbit coupling constant $\zeta = 1333$, and the parameters $\alpha = 19.5$, $\beta = -598, \gamma = 1549$; $P^2 = 253$; $P^4 = 0.5P^2, P^6 = 0.1P^2$,

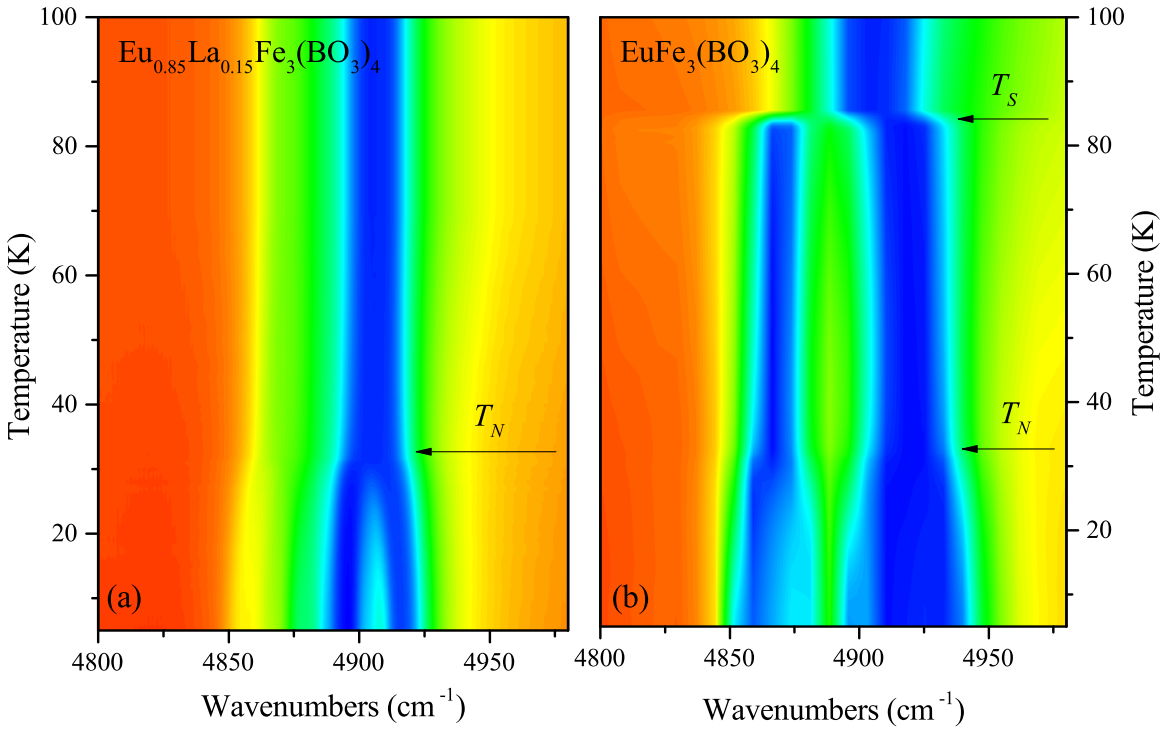

FIG. 6. Intensity maps in the region of the low-frequency part of the ${}^7F_0 \rightarrow {}^7F_6$ optical multiplet of Eu^{3+} in (a) $Eu_{0.85}La_{0.15}Fe_3(BO_3)_4$ and (b) $EuFe_3(BO_3)_4$. Note the absence of a structural phase transition in (a).

$M^0 = 2.39$, $M^2 = 0.56M^0, M^4 = 0.38M^0, T^2 = 376, T^3 = 40, T^4 = 40, T^6 = -330, T^7 = 380, T^8 = 238$ (all the values are in cm^{-1}).

In a local Cartesian system of coordinates with the axes $z||c$, $x||a||C_2$, $y \perp a$, the energy operator of $4f$ electrons in the crystal field has the following form:

$$H_{CF}(D_3) = \sum_j \{B_0^2 C_0^{(2)}(j) + B_0^4 C_0^{(4)}(j) + iB_{-3}^4 [C_{-3}^{(4)}(j) + C_3^{(4)}(j)] + B_0^6 C_0^{(6)}(j) + iB_{-3}^6 [C_{-3}^{(6)}(j) + C_3^{(6)}(j)] + B_6^6 [C_{-6}^{(6)}(j) + C_6^{(6)}(j)]\}, \quad (5)$$

$$\Delta H_{CF}(C_2) = \sum_j \{iB_{-1}^2 [C_{-1}^{(2)}(j) + C_1^{(2)}(j)] + B_2^2 [C_{-2}^{(2)}(j) + C_2^{(2)}(j)] + iB_{-1}^4 [C_{-1}^{(4)}(j) + C_1^{(4)}(j)] + B_2^4 [C_{-2}^{(4)}(j) + C_2^{(4)}(j)] + B_4^4 [C_{-4}^{(4)}(j) + C_4^{(4)}(j)] + iB_{-1}^6 [C_{-1}^{(6)}(j) + C_1^{(6)}(j)] + B_2^6 [C_{-2}^{(6)}(j) + C_2^{(6)}(j)] + B_4^6 [C_{-4}^{(6)}(j) + C_4^{(6)}(j)] + iB_{-5}^6 [C_{-5}^{(6)}(j) + C_5^{(6)}(j)]\}. \quad (6)$$

Here, B_p^q are the crystal-field parameters and $C_p^{(q)}$ are spherical tensor operators.

A. Crystal-field calculations for $EuFe_3(BO_3)_4$ in the $R32$ and $P3_121$ phases

The CF parameters for Eu^{3+} in the $R32$ and $P3_121$ phases of $EuFe_3(BO_3)_4$ were, first, calculated in the frame of the exchange-charge model [40] with making use of the structure parameters of $GdFe_3(BO_3)_4$ from Ref. [2] and, then, corrected by comparing the calculated energies of the CF levels with the experimental optical data. These parameters are given in Table IV. A comparison of the CF parameters determined for different RE ions in RE iron borates [41–44] and presented in Table IV shows an expected monotonous variation due to well-known "lanthanide compression." To account for a low-symmetry quadrupole CF component of the C_2 symmetry, the parameters B_{-1}^2 and B_2^2 obtained earlier from the analysis of the spectra of Tb^{3+} ions in the $TbFe_3(BO_3)_4$ crystal [41] were used.

TABLE IV. Crystal-field parameters $B_p^q(cm^{-1})$ for the R^{3+} ions in $RFe_3(BO_3)_4$ crystals.

q	p	Pr [42] $4f^2$	Nd [43] $4f^3$	Eu (this work) $4f^6$	Tb [41] $4f^8$
2	0	556	551	484	434
4	0	− 1447	− 1239	− 1255	− 1256
6	0	534	519	404	352
4	− 3	867	697	619	608.5
6	− 3	165	105	80	72.6
6	6	376	339	290	270
2	− 1			39	38.4
4	− 1			− 76	− 66
6	− 1			− 32	− 27
2	2			54	54
4	2			102	82
6	2			− 11	− 8.1
4	4			− 26	− 23
6	4			− 31	− 27
6	− 5			− 131	− 91

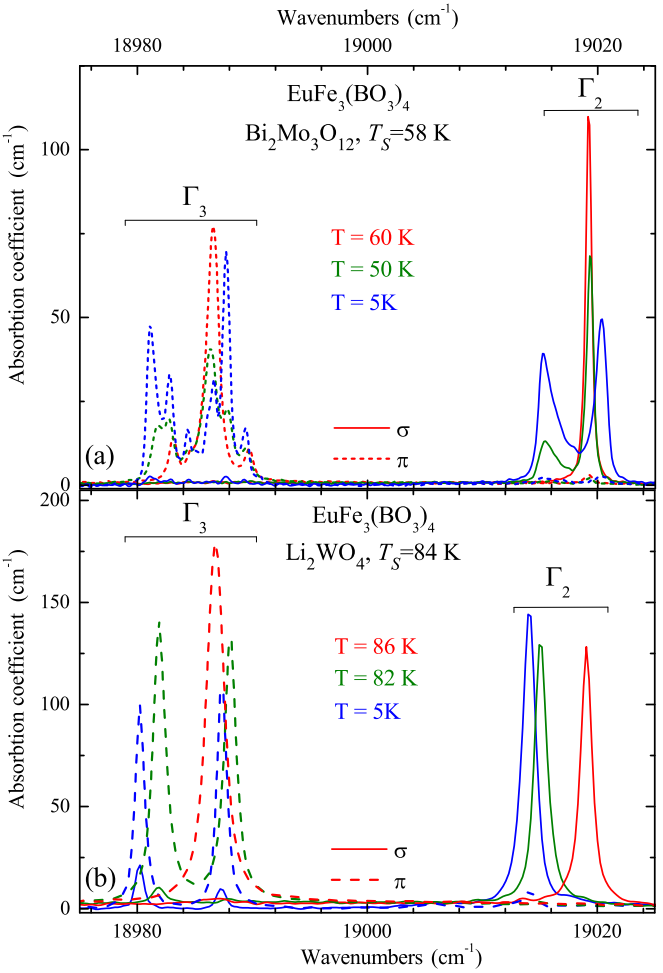

FIG. 7. Absorption spectra in the σ (solid lines) and π (dashed lines) polarizations in the region of the $^7F_0 \rightarrow {}^5D_1$ optical multiplet of Eu^{3+} in $EuFe_3(BO_3)_4$ single crystals grown with (a) $Bi_2Mo_3O_{12}$ and (b) Li_2WO_4 based fluxes, at the three representative temperatures, $T > T_s$ (red traces), $T_s > T > T_N$ (green traces), and $T = 5$ K $< T_N$ (blue traces). Note an enormous difference in T_s for (a) and (b). Multiple extra spectral lines in (a) are due to coexistence of the $P3_121$ and $R32$ phases down to the lowest temperatures.

The energy spectrum and wave functions were calculated by a numerical diagonalization of the operators represented by Eqs. (1)–(3) in a complete basis of the $4f^6$ electronic configuration. The results of calculations are presented in Tables II and V. The second row of Table II gives the irreducible representations that determine symmetry properties of wave functions of the corresponding states in the $R32$ phase. The calculated energies of a majority of CF levels in the $^7F_J (J = 0,1,2,3,4,5,6)$ and $^5D_J (J = 0,1,2)$ multiplets of Eu^{3+} in the $R32$ and $P3_121$ phases of $EuFe_3(BO_3)_4$ (see Table II, rows 5 and 7) satisfactorily agree with measurement data (rows 4 and 6). We note that the measured spectra of the europium ions in isostructural crystals of aluminum and iron borates (Table II, rows 3 and 4, respectively) are similar, with an exception of positions of several levels (marked by footnote *b*), assignments of which in Ref. [45] have to be checked. Errors in the interpretation of corresponding spectral lines resulted in a qualitatively different set of CF parameters in Ref. [45].

In Table V, measured and calculated splittings of Γ_3 non-Kramers doublets at the $R32 \rightarrow P3_121$ symmetry lowering are listed. There is a satisfactory agreement between the calculated and measured values, with the exception of the $3\Gamma_3(^7F_4)$ level, where the calculated splitting is 3.5 times smaller than the measured one. One can conclude from the results of measurements and calculations that splittings of different Γ_3 doublets differ by more than an order of magnitude (see Tables II and V).

B. Calculations of the Eu^{3+} spectra in a magnetically ordered $EuFe_3(BO_3)_4$

The spectra of the Eu^{3+} ions in the antiferromagnetic collinear phase were calculated assuming a dominant role of the isotropic component in the exchange interaction between the europium ions and the six neighboring iron ions. The *f-d* exchange interaction between a Eu^{3+} ion and a Fe^{3+} ion has the form $H_{\mathrm{Eu-Fe}} = -2J_{fd}\mathbf{S}_{\mathrm{Eu}}\mathbf{S}_{\mathrm{Fe}}$, where S_{Eu} and S_{Fe} are operators of the corresponding spin moments. In this case, an effective exchange Hamiltonian for the Eu^{3+} ions reads

$$H_{fd} = -12J_{fd} < S_{\mathrm{Fe}} > S_{\mathrm{Eu},x} \qquad (7)$$

(for the Eu^{3+} ions EuI with the local x axis parallel to iron magnetic moments), or

$$H_{fd} = -6J_{fd} < S_{\mathrm{Fe}} > (\pm\sqrt{3}S_{\mathrm{Eu},y} - S_{\mathrm{Eu},x}) \qquad (8)$$

(for the Eu^{3+} ions EuII having the local x axis at the angle $\pm 2\pi/3$ with the direction of the iron magnetic moments). In the present work, we neglect a possible magnetic anisotropy of the iron ions and differences between magnetic characteristics of the Fe^{3+} ions occupying crystallographically nonequivalent sites Fe(I) and Fe(II) in the low-temperature $P3_121$ phase [2].

Because all CF energy levels of the Eu^{3+} ions are nondegenerate in the $P3_121$ phase, a magnetic ordering of the Fe^{3+} ions induces only relatively small shifts of the spectral lines. In particular, according to the selection rules for the magnetic dipole transitions in Table I, matrix elements of the europium spin operator $S_{\mathrm{Eu},x}$ (which transforms like μ_x) are nonzero between the states corresponding to the same irreducible representation, γ_1 or γ_2. So, in the spectrum of the EuI ions, shifts of Γ_3 doublet's sublevels γ_1 and γ_2 can be induced only by a mixing of their wave functions with those of the nearest singlets. In the case of the EuII ions, shifts of Γ_3 doublet's sublevels are governed by matrix elements of the europium spin moment $S_{\mathrm{Eu},y}$ given in Table V, however, an additional splitting in the magnetically ordered phase strongly depends on the gap between these sublevels induced by the low-symmetry CF component in the $P3_121$ phase.

Calculations of the spectra of nonequivalent europium ions were performed using the value of the exchange integral $J_{fd} = 0.26$ K obtained earlier from the analysis of the low-temperature spectra of a $TbFe_3(BO_3)_4$ crystal [41]. The results of the calculations are compared with the experimental data in Table III. There is a correlation between the largest values of matrix elements of the $S_{\mathrm{Eu},y}$ operator given in Table V and the biggest shifts of the corresponding energy levels. Calculations of the Eu^{3+} spectra in a magnetically ordered $EuFe_3(BO_3)_4$

TABLE V. Splittings of the Γ_3 doublets in the $P3_121$ phase and their magnetic spectroscopic factors.

Doublets in the $R32$ phase		g factors g_{zz}	Splitting of the doublet in the $P3_121$ phase (cm^{-1})		$2\lvert\langle\Gamma_3 1\rvert S_y\rvert\Gamma_3 2\rangle\rvert$
			Measured	Calculated	
$^7F_1$	Γ_3	3.37	24	27	0.102
$^7F_2$	$1\Gamma_3$	0.97		4.5	0.076
	$2\Gamma_3$	3.12		10.2	0.132
$^7F_3$	$1\Gamma_3$	1.12	7	4.7	0.646
	$2\Gamma_3$	4.82		15.2	0.119
$^7F_4$	$1\Gamma_3$	8.89	62	34.4	0.043
	$2\Gamma_3$	3.88	74	51.1	0.783
	$3\Gamma_3$	4.51	27	7.6	0.542
$^7F_5$	$1\Gamma_3$	0.36		14.3	1.130
	$2\Gamma_3$	12.56		4.9	1.114
	$3\Gamma_3$	5.15		5.3	0.330
	$4\Gamma_3$	11.46		1.6	0.056
$^7F_6$	$1\Gamma_3$	8.34		1.8	4.336
	$2\Gamma_3$	7.02		3.8	1.186
	$3\Gamma_3$	5.67	34	35.2	0.359
	$4\Gamma_3$	12.74		2.9	0.084
$^5D_1$	Γ_3	3.02	6	7.0	0.078
$^5D_2$	$1\Gamma_3$	4.90	1	1	0.106
	$2\Gamma_3$	1.81	4	7.0	0.022

confirm the interpretation of an additional splitting of spectral lines observed below T_N as originating from nonequivalent europium positions that appear in the case of iron magnetic moments collinear with one of the C_2 axes.

The above presented results of the analysis of spectral characteristics of the europium ions can be used to interpret earlier published data on the magnetic susceptibility, magnetization, and magnetic-field-induced electric polarization of $EuFe_3(BO_3)_4$ [6,8,23].

C. Modeling of the magnetic susceptibility and electric polarization of $EuFe_3(BO_3)_4$

When analyzing the magnetic properties of $EuFe_3(BO_3)_4$ in the external magnetic field $\boldsymbol{B}$, we add to the effective Hamiltonian of a single Eu^{3+} ion [see Eqs. (1)–(3)] the energy of the Zeeman interaction $H_Z = \mu_B \boldsymbol{m}\boldsymbol{B}$, where μ_B is the Bohr magneton, $\boldsymbol{m} = \sum_j (\boldsymbol{l}_j + 2\boldsymbol{s}_j)$, and we use the values of the magnetic order parameter $\langle S_{Fe,x}\rangle$ presented versus temperature below T_N in Ref. [46]. Temperature dependencies of the europium magnetic moments induced by the external magnetic field and the exchange interaction were obtained using a numerical procedure of the quantum-statistical averaging with a step of 1 K. In particular, the calculated magnetic moments in zero external field at the temperature 5 K, induced by the exchange field ($\langle S_{Fe,x}\rangle = 2.4$), equal 0.117 μ_B and are parallel to the a axis for the EuI sites and equal 0.13 μ_B, being declined from the a axis in the ab plane by the angles $\pm 63^\circ$, for the EuII sites.

Temperature dependencies of the magnetic susceptibilities of Eu^{3+} ions presented in Fig. 8 (inset) were obtained from calculations of the average magnetic moments induced by the external magnetic field $B = 0.1$ T in the paramagnetic $R32$ and $P3_121$ phases, as well as in the antiferromagnetic phase in the presence of a nonzero exchange interaction (7) and (8). The transverse Van Vleck susceptibility $\chi_{Eu,\perp} = (\chi_{Eu,xx} + \chi_{Eu,yy})/2$ increases monotonely with decreasing temperature; a nonmonotonic variation of the longitudinal susceptibility $\chi_{Eu,||}$ with a broad maximum at about 180 K is caused by a paramagnetic contribution from the first excited non-Kramers doublet in the $^7F_1$ multiplet. Despite relatively

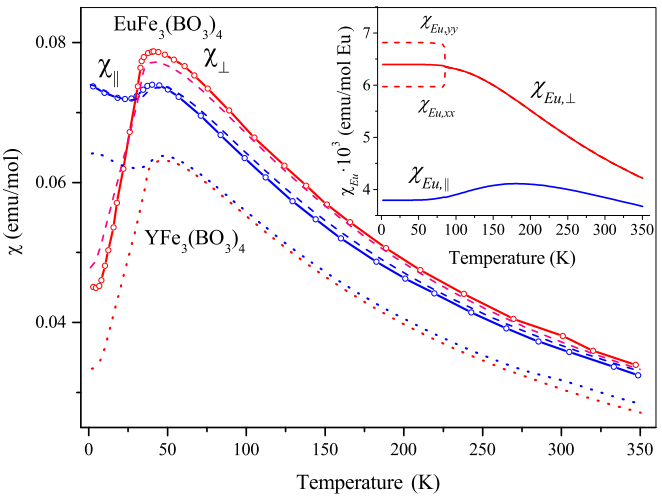

FIG. 8. Temperature dependencies of the magnetic susceptibilities of $EuFe_3(BO_3)_4$ (experimental data [6] are presented by lines with symbols, dashed lines represent the results of simulations) and $YFe_3(BO_3)_4$ (dotted lines, from Ref. [46]) in magnetic fields $B = 0.1$ T parallel and normal to the c axis. Inset: calculated single Eu^{3+} ion susceptibilities; at temperatures below T_s the susceptibilities in magnetic fields along and normal to the C_2 axis become different (dashed lines), however, their average as well as the susceptibility along the c axis show only negligible discontinuities.

large discontinuities of different signs in $\chi_{\mathrm{Eu},xx}$ and $\chi_{\mathrm{Eu},yy}$ at the structural transition $R32 \rightarrow P3_121$, the calculated transverse and longitudinal susceptibilities do not show any noticeable peculiarities at temperatures close to T_s. Because of small magnetic moments in the magnetically ordered phase and weak responses of the Eu^{3+} ions on external fields, one may expect only weak renormalization of the susceptibilities of the europium and iron subsystems. Indeed, a comparison of the temperature dependencies of the susceptibilities of the europium and yttrium iron borates measured in Refs. [6,46], respectively, demonstrates a very similar behavior (see Fig. 8). Note that $YFe_3(BO_3)_4$ contains only one magnetic system of Fe^{3+} ions and, due to slightly larger exchange interactions between the iron ions because of shorter interion distances, has a slightly higher temperature of the magnetic phase transition, $T_N = 37$ K. Accordingly, curves reproducing the susceptibilities of the europium borate with $T_N = 34$ K are shifted by about 3–4 K to lower temperatures relative to the ones presenting susceptibilities of the yttrium borate. Besides, in the total temperature range 2–350 K, the susceptibilities of the europium borate contain an additional approximately constant pedestal that corresponds to the contribution of the Eu^{3+} ions.

However, the sums of the calculated susceptibilities of the Eu^{3+} ions and the measured susceptibilities of the Fe^{3+} ions in yttrium borate are still markedly less than the experimental data for $EuFe_3(BO_3)_4$. We have carried out more detailed simulations in the framework of an approach derived earlier to model magnetic properties of other iron borates [41–44]. This approach is based on the analytical expression for the susceptibility χ_{Fe} of the Fe^{3+} ions coupled by the isotropic antiferromagnetic exchange interactions with their nearest neighbors within the helical chains and in the two adjacent chains [see Eq. (8) in Ref. [43]]. To account for the *f-d* exchange interactions, for example, in the paramagnetic $R32$ phase, we consider the following perturbation Hamiltonian of a single Eu^{3+} ion:

$$\Delta H = \mu_B \boldsymbol{m}\boldsymbol{B} + \mu_B \boldsymbol{S}_{\mathrm{Eu}} \boldsymbol{B}_{ex}, \tag{9}$$

and calculate, besides the components of the susceptibility tensor χ_{Eu}, the temperature dependencies of the tensors $\boldsymbol{\beta}$, $\boldsymbol{\gamma}$, and $\boldsymbol{\delta}$, which determine linear responses of the average magnetic and spin moments of the Eu^{3+} ions to the external ($\boldsymbol{B}$) and exchange ($B_{ex} = 3\lambda_{fd}\langle M_{Fe}\rangle, \lambda_{\mathrm{fd}} = 2J_{\mathrm{fd}}/{\mu_B}^2$) fields:

$$-\mu_B\langle \boldsymbol{m}\rangle = \chi_{\mathrm{Eu}}\boldsymbol{B} + \delta \boldsymbol{B}_{ex}, \tag{10}$$

$$-\mu_B\langle \boldsymbol{S}_{\mathrm{Eu}}\rangle = \beta \boldsymbol{B} + \gamma \boldsymbol{B}_{ex}. \tag{11}$$

From Eqs. (10) and (11) and the expression for the average iron magnetic moment

$$\langle \boldsymbol{M}_{\mathrm{Fe}}\rangle = -2\mu_B\langle \boldsymbol{S}_{\mathrm{Fe}}\rangle = \chi_{\mathrm{Fe}}(\boldsymbol{B} - \lambda_{fd}\mu_B\langle \boldsymbol{S}_{\mathrm{Eu}}\rangle), \tag{12}$$

it is easy to obtain components of the bulk susceptibility tensor (N_A is the Avogadro number):

$$\chi_{\alpha\alpha} = N_A\left[\chi_{\mathrm{Eu},\alpha\alpha} + 3\chi_{\mathrm{Fe}}\frac{(1+\lambda_{fd}\beta_{\alpha\alpha})(1+\lambda_{fd}\delta_{\alpha\alpha})}{1-3\lambda_{fd}^2\chi_{\mathrm{Fe}}\gamma_{\alpha\alpha}}\right]. \tag{13}$$

A similar procedure was carried out to obtain expressions for the susceptibilities in the $P3_121$ phase [41]. Numerical calculations were fulfilled using values of the exchange interaction parameters close to the ones presented earlier in Refs. [41–44]: $J_{fd} = +0.26$ K (a positive sign means that magnetic moments of the Eu^{3+} ion and the nearest six Fe^{3+} ions are coupled ferromagnetically), and $J_{nn} = -6.75$ K, $J_{nnn} = -1.9$ K for the intra- and interchain interactions between the iron ions. As is seen in Fig. 8, the results of simulations match satisfactorily the experimental data. A successful analysis of the magnetic susceptibilities brings an additional confidence in a real physical meaning of the crystal-field and exchange parameters of $EuFe_3(BO_3)_4$ obtained in the present work.

Having in hand all parameters which determine the electronic structure of the Eu^{3+} ions, we are able to estimate the contribution of the europium subsystem into the electric polarization induced by an external magnetic field. In the present study, we confine ourselves to a consideration of the $R32$ phase; the $P3_121$ one requires cumbersome calculations, which will be a subject of a separate work. We follow the approach developed in Ref. [21], however, without using any fitting parameters. In the $R32$ phase, components of the effective electric dipolar moment of a rare-earth ion in iron borates are presented by the following operators determined in the space of the electronic $4f$ states:

$$D_\alpha = \frac{e r_{fd}}{W_{5d,4f}}\sum_j \sum_{\substack{p=2,4,6\\ 2\leqslant k\leqslant p}} \left(b^p_{k,\alpha}B^3_3 + d^p_{k,\alpha}B^5_3\right) \left[C^{(p)}_{-k}(j) + \varepsilon_\alpha C^{(p)}_k(j)\right], \tag{14}$$

where e is the elementary charge, $r_{fd} = 0.35$ Å [47] is the radial integral, $W_{5d,4f} = 6\times10^4$ cm^{-1} is the energy of Eu^{3+} ion excitation from the ground state to the $4f^5 5d$ configuration, $\varepsilon_x = 1$, $\varepsilon_y = \varepsilon_z = -1$, $B^3_3 = 2110$ cm^{-1} and $B^5_3 = 2170$ cm^{-1} are parameters of the odd CF Hamiltonian [42]; the corrected values of the nonzero dimensionless coefficients (as compared with Ref. [21]) are $b^2_{2,x} = 2\sqrt{30}/49$, $b^4_{2,x} = -11\sqrt{2}/98$, $b^4_{4,x} = 11\sqrt{14}/49$, $b^4_{3,z} = 11\sqrt{7}/49$, $d^4_{2,x} = 2\sqrt{14}/77$, $d^4_{4,x} = -\sqrt{2}/77$, $d^6_{4,x} = 39\sqrt{10}/154$ $b^p_{2,y} = -ib^p_2$, $b^p_{4,y} = ib^p_{4,x}$, $d^p_{2,y} = -id^p_{2,x}$, $d^p_{4,y} = id^p_{4,x}$, $d^4_{3,z} = 8/77$, $d^6_{3,z} = 39\sqrt{10}/77$. To evaluate the ionic contribution into the polarization, we considered a shift δx of the europium sublattices along the a axis. Parameters of the corresponding additional term in the CF Hamiltonian for the Eu^{3+} ions, $\delta H_{CF} = V\delta x$, $V = \sum_j\sum_{p,k} v^p_k[C^{(p)}_{-k}(j) + C^{(p)}_k(j)]$, $v^2_2 = -2950$, $v^4_2 = -2675$, $v^6_2 = 620$, $v^4_4 = 295$, $v^6_4 = -16$, $v^6_5 = -947i$ (cm^{-1}/Å), were calculated in the framework of the exchange-charge model [40].

The computed values of the electronic ($P^e_a = 3\langle D_x\rangle/v$) and ionic ($P^i_a = -9e\langle V\rangle/Kv$) polarizations induced by an external magnetic field $B\perp c$ in the paramagnetic phase having the $R32$ crystal structure satisfy a relation $P_a \sim B^2_x - B^2_y$ imposed by the local D_3 symmetry at Eu sites. Here $v = a_0^2 c_0\sqrt{3}/2$ (a_0 and c_0 are lattice constants) is the unit-cell volume containing three Eu^{3+} ions, $K = m_{\mathrm{Eu}}\omega^2$ is the force constant corresponding to vibrations of Eu^{3+} ions

with the frequency $\omega/2\pi c = 116\ \mathrm{cm}^{-1}$ estimated according to Ref. [48], $\langle \ldots \rangle$ means averaging with the equilibrium density matrix corresponding to the single-ion Hamiltonian $H = H_{FI} + H_{CF}(D_3) - 12J_{fd}\langle \mathbf{S}_{\mathrm{Fe}} \rangle \mathbf{S}_{\mathrm{Eu}} + H_Z$. However, the obtained values of both electronic and ionic polarizations of the europium subsystem in the $R32$ phase differ in sign and magnitude from the measured data. Results of the field-induced polarization $P_a(T)$ measurements for $EuFe_3(BO_3)_4$ in the temperature interval 40–170 K (that includes the $R32$ phase) under magnetic fields $B_a = 5$ and 10 T are given in Ref. [6]. In this range of temperatures, $P_a < 0$, the absolute value of P_a gradually grows with lowering the temperature, reaches a maximum at $T_s \approx 60$ K and then diminishes again. Under $B_a = 10$ T, the measured values of polarization are $P_a(100\ \mathrm{K}) = P_a(40\ \mathrm{K}) = -10\,\mu\mathrm{C/m}^2$ [6], whereas our calculated values ($B_a = 10$ T, $T = 100$ K) are $P_a^e = 0.073\,\mu\mathrm{C/m}^2$ and $P_a^i = 0.657\,\mu\mathrm{C/m}^2$. Here we should note that for temperatures below T_s (the $P3_121$ phase), where a comparison can be made between the experimental data of Refs. [6] and [8], Ref. [6] reports P_a values, the moduli of which are of about an order of magnitude higher than those reported in Ref. [8]. The reason for such a discrepancy has to be analyzed. The main conclusion that follows from our calculations is that one can neglect a direct contribution of $4f$ electrons (P_a^e) into the formation of a magnetoelectric response of RE borates with huntite structure. As for the ionic mechanism, a more elaborate study is necessary, accounting for the CF and anisotropic f-d exchange modulations by relative shifts of the rare-earth, iron, and oxygen sublattices.

VI. CONCLUSION

In summary, we have performed a thorough high-resolution temperature-dependent polarized optical spectroscopy study of multiferroic $EuFe_3(BO_3)_4$ single crystals in the three phases, namely, in the paramagnetic $R32$ ($T > T_s = 84$ K) and $P3_121$ ($T_s > T > T_N = 34$ K) phases and the antiferromagnetic one ($T < T_N$). From the spectra analysis, positions and symmetries of 24 and 38 CF levels of Eu^{3+} in the high-temperature $R32$ and low-temperature $P3_121$ phases, respectively, were reliably determined. The most important result was obtained when analyzing the spectral data for the magnetically ordered phase. A well resolved splitting of spectral lines corresponding to singlet-singlet optical transitions into doublets with the ratio 1:2 for intensities of the doublet's components is in agreement with a collinear ordering of iron magnetic moments along one of the three C_2 axes and results from magnetically nonequivalent europium ions.

Crystal-field calculations were performed, starting from the CF parameters obtained in the frame of the exchange-charge model, with a subsequent correction by comparing the calculated energies of the Eu^{3+} CF levels with the experimental optical data. Calculations of the spectra of nonequivalent europium ions in the magnetically ordered phase of $EuFe_3(BO_3)_4$ were carried out assuming an isotropic exchange interaction between a europium ion and the six neighboring iron ions and using the value of the exchange integral $J_{fd} = 0.26$ K. These calculations strongly support our conclusion, based on the high-resolution spectra, about a collinear structure of iron magnetic moments along one of the three C_2 axes. Crystal-field and exchange parameters were further used to calculate the magnetic susceptibility of the $EuFe_3(BO_3)_4$ single crystal in the frame of a model that takes into account a strong interaction of iron ions within the -Fe-O-Fe- chains in the structure by considering dimers composed of neighboring iron ions in the chain. Averaging over the three types of magnetic domains corresponding to the three equivalent C_2 axes was performed. A good agreement with the experimental data from literature was obtained. An important result of the present study is that it has delivered physically grounded crystal-field parameters for $EuFe_3(BO_3)_4$, which can be used for interpreting magnetic, magnetoelectric, and other properties of this multiferroic compound. The calculated contributions of the electronic $4f$ shell of the Eu^{3+} ions into the electric polarization of $EuFe_3(BO_3)_4$ in the $R32$ phase induced by external magnetic fields are negligible as compared to the measured values. An order of magnitude larger polarization is obtained from calculations of the shifts of the europium sublattices in an external magnetic field but it still differs from the measured values, at least in sign. Thus, more detailed studies of the interaction between the Eu^{3+} ions and optical phonons active in the infrared lattice absorption are necessary to determine unambiguously the most efficient mechanism of the magnetoelectric coupling.

Furthermore, our study has revealed peculiarities in structural and optical properties of $EuFe_3(BO_3)_4$, connected with a method of the crystal growth. We emphasize an importance of paying attention to growth-method-dependent special features of functional RE borates, when treating their optical, magnetic, and magnetoelectric properties. We have demonstrated a suppression of the $R32 \rightarrow P3_121$ structural phase transition in the $Eu_{0.85}La_{0.15}Fe_3(BO_3)_4$ crystal and a possibility to control the temperature of the structural phase transition in RE iron borates, which implies an application potential.

ACKNOWLEDGMENTS

This work was supported by the Russian Science Foundation under Grant No. 14-12-01033. I.A.G. and V.L.T. are grateful to L. N. Bezmaternykh for useful comments concerning the crystal growth, to M. S. Molokeev for the XRD characterization of the samples, and to the Russian Foundation for Basic Research for a financial support (Grants No. 13-02-12442 and No. 14-02-00307a).

[1] N. I. Leonyuk and L. I. Leonyuk, Prog. Cryst. Growth Charact. Mater. **31**, 179 (1995).

[2] S. A. Klimin, D. Fausti, A. Meetsma, L. N. Bezmaternykh, P. H. M. van Loosdrecht, and T. T. M. Palstra, Acta Crystallogr., Sect. B: Struct. Sci. **61**, 481 (2005).

[3] A. M. Kalashnikova, V. V. Pavlov, R. V. Pisarev, L. N. Bezmaternykh, M. Bayer, and Th. Rasing, JETP Lett. **80**, 293 (2004).

[4] Ph. Goldner, O. Guillot-Noel, J. Petit, M. Popova, and L. Bezmaternykh, Phys. Rev. B **76**, 165102 (2007).

[5] Y. Hinatsu, Y. Doi, K. Ito, M. Wakeshima, and A. Alemi, J. Solid State Chem. **172**, 438 (2003).

[6] A. M. Kadomtseva, Yu. F. Popov, G. P. Vorob'ev, A. P. Pyatakov, S. S. Krotov, K. I. Kamilov, V. Yu. Ivanov, A. A. Mukhin, A. K. Zvezdin, A. M. Kuz'menko, L. N. Bezmaternykh, I. A. Gudim, and V. L. Temerov, Low Temp. Phys. **36**, 511 (2010).

[7] R. P. Chaudhury, F. Yen, B. Lorenz, Y. Y. Sun, L. N. Bezmaternykh, V. L. Temerov, and C. W. Chu, Phys. Rev. B **80**, 104424 (2009).

[8] T. Kurumaji, K. Ohgushi, and Y. Tokura, Phys. Rev. B **89**, 195126 (2014).

[9] H. J. Zhao, Y. Yang, W. Ren, A.-J. Mao, X. M. Chen, and L. Bellaiche, J. Phys.: Condens. Matter **26**, 472201 (2014).

[10] K.-C. Liang, R. P. Chaudhury, B. Lorenz, Y. Y. Sun, L. N. Bezmaternykh, V. L. Temerov, and C. W. Chu, Phys. Rev. B **83**, 180417(R) (2011).

[11] N. V. Volkov, I. A. Gudim, E. V. Eremin, A. I. Begunov, A. A. Demidov, and K. N. Boldyrev, JETP Lett. **99**, 67 (2014).

[12] F. Yen, B. Lorenz, Y. Y. Sun, C. W. Chu, L. N. Bezmaternykh, and A. N. Vasiliev, Phys. Rev. B **73**, 054435 (2006).

[13] U. Adem, L. Wang, D. Fausti, W. Schottenhamel, P. H. M. van Loosdrecht, A. Vasiliev, L. N. Bezmaternykh, B. Buchner, C. Hess, and R. Klingeler, Phys. Rev. B **82**, 064406 (2010).

[14] A. A. Mukhin, G. P. Vorob'ev, V. Yu. Ivanov, A. M. Kadomtseva, A. S. Narizhnaya, A. M. Kuz'menko, Yu. F. Popov, L. N. Bezmaternykh, and I. A. Gudim, JETP Lett. **93**, 275 (2011).

[15] E. Bovero, Z. D. Luo, Y. D. Huang, A. Benayas, and D. Jaque, Appl. Phys. Lett. **87**, 211108 (2005).

[16] J. M. Dawes, P. Dekker, Ph. Burns, and J. A. Piper, Opt. Rev. **12**, 101 (2005).

[17] K. N. Gorbachenya, V. E. Kisel, A. S. Yasukevich, V. V. Maltsev, N. I. Leonyuk, and N. V. Kuleshov, Opt. Lett. **41**, 918 (2016).

[18] A. K. Zvezdin, G. P. Vorob'ev, A. M. Kadomtseva, Yu. F. Popov, A. P. Pyatakov, L. N. Bezmaternykh, A. V. Kuvardin, and E. A. Popova, JETP Lett. **83**, 509 (2006).

[19] Yu. F. Popov, A. P. Pyatakov, A. M. Kadomtseva, G. P. Vorob'ev, A. K. Zvezdin, A. A. Mukhin, V. Yu. Ivanov, and I .A. Gudim, JETP **111**, 199 (2010).

[20] A. K. Zvezdin, A. M. Kadomtseva, Yu. F. Popov, G. P. Vorob'ev, A. P. Pyatakov, V. Yu. Ivanov, A. M. Kuz'menko, A. A. Mukhin, L. N. Bezmaternykh, and I. A. Gudim, JETP **109**, 68 (2009).

[21] A. I. Popov, D. I. Plokhov, and A. K. Zvezdin, Phys. Rev. B **87**, 024413 (2013).

[22] N. V. Kostyuchenko, A. I. Popov, and A. K. Zvezdin, Fiz. Tverd. Tela **54**, 1493 (2012) [Phys. Solid State **54**, 1591 (2012)].

[23] V. P. Dyakonov, R. Szymczak, A. D. Prokhorov, E. Zubov, A. A. Prokhorov, G. Petrakovskii, L. Bezmaternikh, M. Berkowski, V. Varyukhin, and H. Szymczak, Eur. Phys. J. B **78**, 291 (2010).

[24] D. Fausti, A. A. Nugroho, P. H. M. van Loosdrecht, S. A. Klimin, M. N. Popova, and L. N. Bezmaternykh, Phys. Rev. B **74**, 024403 (2006).

[25] K. N. Boldyrev, T. N. Stanislavchuk, S. A. Klimin, M. N. Popova, and L. N. Bezmaternykh, Phys. Lett. A **376**, 2562 (2012).

[26] C. Ritter, A. Vorotynov, A. Pankrats, G. Petrakovskii, V. Temerov, I. Gudim, and R. Szymczak, J. Phys.: Condens. Matter **20**, 365209 (2008).

[27] C. Ritter, A. Vorotynov, A. Pankrats, G. Petrakovskii, V. Temerov, I. Gudim, and R. Szymczak, J. Phys.: Condens. Matter **22**, 206002 (2010).

[28] M. Janoschek, P. Fischer, J. Schefer, B. Roessli, V. Pomjakushin, M. Meven, V. Petricek, G. Petrakovskii, and L. Bezmaternikh, Phys. Rev. B **81**, 094429 (2010).

[29] M. N. Popova, J. Appl. Phys. **76**, 7105 (1994).

[30] I. V. Golosovsky, V. P. Plakhty, V. P. Harchenkov, S. V. Sharigin, and J. Schweizer, J. Magn. Magn. Mater. **129**, 233 (1994).

[31] M. N. Popova and I. V. Paukov, Opt. Spectrosc. **76**, 254 (1994).

[32] I. A. Gudim, E. V. Eremin, and V. L. Temerov, J. Crystal Growth **312**, 2427 (2010).

[33] K. N. Boldyrev, M. N. Popova, M. Bettinelli, V. L. Temerov, I. A. Gudim, L. N. Bezmaternykh, P. Loiseau, G. Aka, and N. I. Leonyuk. Opt. Mater. **34**, 1885 (2012).

[34] K. V. Frolova, I. S. Lyubutin, E. S. Smirnova, O. A. Alekseeva, I. A. Verin, V. V. Artemov, S. A. Kharlamova, L. N. Bezmaternykh, and I. A. Gudim, J. Alloys Compd. **671**, 545 (2016).

[35] S. A. Klimin, A. B. Kuzmenko, M. A. Kashchenko, and M. N. Popova, Phys. Rev. B **93**, 054304 (2016).

[36] R. V. Pisarev, M. A. Prosnikov, V. Yu. Davydov, A. N. Smirnov, E. M. Roginskii, K. N. Boldyrev, A. D. Molchanova, M. N. Popova, M. B. Smirnov, and V. Yu. Kazimirov, Phys. Rev. B **93**, 134306 (2016).

[37] D. A. Erofeev, E. P. Chukalina, L. N. Bezmaternykh, I. A. Gudim, and M. N. Popova, Opt. Spectrosc. **120**, 558 (2016).

[38] R. D. Shannon, Acta Crystallogr., Sect. A: Cryst. Phys., Diffr., Theor. Gen. Crystallogr. **32**, 751 (1976).

[39] W. T. Carnall, G. L. Goodman, K. Rajnak, and R. S. Rana, J. Chem. Phys. **90**, 3443 (1989).

[40] B. Z. Malkin, in *Spectroscopy of Solids Contaning Rare Earth Ions*, edited by A. A. Kaplyanskii and R. M. Macfarlane (North-Holland, Amsterdam, 1987), Chap. 2, pp. 13–50.

[41] M. N. Popova, T. N. Stanislavchuk, B. Z. Malkin, and L. N. Bezmaternykh, J. Phys.: Condens. Matter **24**, 196002 (2012).

[42] M. N. Popova, T. N. Stanislavchuk, B. Z. Malkin, and L. N. Bezmaternykh, Phys. Rev. B **80**, 195101 (2009).

[43] M. N. Popova, E. P. Chukalina, T. N. Stanislavchuk, B. Z. Malkin, A. R. Zakirov, E. Antic-Fidancev, E. A. Popova, L. N. Bezmaternykh, and V. L. Temerov, Phys. Rev. B **75**, 224435 (2007).

[44] M. N. Popova, E. P. Chukalina, B. Z. Malkin, D. A. Erofeev, L. N. Bezmaternykh, and I. A. Gudim, JETP **118**, 111 (2014).

[45] C. Gorller-Walrand, P. Vandevelde, I. Hendrickx, P. Porcher, J. C. Krupa, and G. S. D. King, Inorg. Chim. Acta **143**, 259 (1988).

[46] E. A. Popova, A. N. Vasiliev, V. L. Temerov, L. N. Bezmaternykh, N. Tristan, R. Klingeler, and B. Büchner, J. Phys.: Condens. Matter **22**, 116006 (2010).

[47] G. W. Burdick and M. F. Reid, in *Handbook on the Physics and Chemistry of Rare Earths* (Elsevier, New York, 2007), Vol. 37, Chap. 232, pp. 61–98.

[48] K. Papagelis, J. Arvanitidis, G. Kanellis, S. Ves, and G. A. Kourouklis, J. Phys.: Condens. Matter **14**, 3875 (2002).